

Spontaneous isospin polarization and quantum Hall ferromagnetism in a rhombohedral trilayer graphene superlattice

Xiangyan Han(韩香岩), Qianling Liu(刘倩伶), Ruirui Niu(牛锐锐), Zhuangzhuang Qu(曲壮壮), Zhiyu Wang(王知雨), Zhuoxian Li(李卓贤), Chunrui Han(韩春蕊), Kenji Watanabe, Takashi Taniguchi, Zizhao Gan(甘子钊), and Jianming Lu(路建明)

Citation: Chin. Phys. B, 2023, 32 (**11**): 117201. DOI: 10.1088/1674-1056/acddcf
Journal homepage: http://cpb.iphy.ac.cn; http://iopscience.iop.org/cpb

What follows is a list of articles you may be interested in

Emergence of correlations in twisted monolayer-trilayer graphene heterostructures

Zhang Zhou(周璋), Kenji Watanabe, Takashi Taniguchi, Xiao Lin(林晓), Jinhai Mao(毛金海), and Hong-Jun Gao(高鸿钧)

Chin. Phys. B, 2023, 32 (**9**): 097203. DOI: 10.1088/1674-1056/ace3a8

Tunable correlation in twisted monolayer-trilayer graphene

Dongdong Ding(丁冬冬), Ruirui Niu(牛锐锐), Xiangyan Han(韩香岩), Zhuangzhuang Qu(曲壮壮), Zhiyu Wang(王知雨), Zhuoxian Li(李卓贤), Qianling Liu(刘倩伶), Chunrui Han(韩春蕊), and Jianming Lu(路建明)

Chin. Phys. B, 2023, 32 (**6**): 067204. DOI: 10.1088/1674-1056/acc8c3

Correlated states in alternating twisted bilayer-monolayer-monolayer graphene heterostructure

Ruirui Niu(牛锐锐), Xiangyan Han(韩香岩), Zhuangzhuang Qu(曲壮壮), Zhiyu Wang(王知雨), Zhuoxian Li(李卓贤), Qianling Liu(刘倩伶), Chunrui Han(韩春蕊), and Jianming Lu(路建明)

Chin. Phys. B, 2023, 32 (**1**): 017202. DOI: 10.1088/1674-1056/ac9de4

Strain-dependent resistance and giant gauge factor in monolayer WSe_2

Mao-Sen Qin(秦茂森), Xing-Guo Ye(叶兴国), Peng-Fei Zhu(朱鹏飞), Wen-Zheng Xu(徐文正), Jing Liang(梁晶), Kaihui Liu(刘开辉), and Zhi-Min Liao(廖志敏)

Chin. Phys. B, 2021, 30 (**9**): 097203. DOI: 10.1088/1674-1056/ac11d2

Mobility edges and reentrant localization in one-dimensional dimerized non-Hermitian quasiperiodic lattice

Xiang-Ping Jiang(蒋相平), Yi Qiao(乔艺), and Jun-Peng Cao(曹俊鹏)

Chin. Phys. B, 2021, 30 (**9**): 097202. DOI: 10.1088/1674-1056/ac11e5

Spontaneous isospin polarization and quantum Hall ferromagnetism in a rhombohedral trilayer graphene superlattice

Xiangyan Han(韩香岩)[1], Qianling Liu(刘倩伶)[1], Ruirui Niu(牛锐锐)[1], Zhuangzhuang Qu(曲壮壮)[1], Zhiyu Wang(王知雨)[1], Zhuoxian Li(李卓贤)[1], Chunrui Han(韩春蕊)[2,3,†], Kenji Watanabe[4], Takashi Taniguchi[4], Zizhao Gan(甘子钊)[1], and Jianming Lu(路建明)[1,‡]

[1] *State Key Laboratory for Mesoscopic Physics, School of Physics, Peking University, Beijing* 100871, *China*
[2] *Institute of Microelectronics, Chinese Academy of Sciences, Beijing* 100029, *China*
[3] *University of Chinese Academy of Sciences, Beijing* 100049, *China*
[4] *National Institute for Materials Science*, 1-1 *Namiki, Tsukuba*, 305-0044, *Japan*

(Received 12 April 2023; revised manuscript received 8 June 2023; accepted manuscript online 13 June 2023)

Moiré superlattices in van der Waals heterostructures have recently attracted enormous interests, due to the highly controllable electronic correlation that gives rise to superconductivity, ferromagnetism, and nontrivial topological properties. To gain a deep understanding of such exotic properties, it is essential to clarify the broken symmetry between spin and valley flavors which universally exists in these ground states. Here in a rhombohedral trilayer graphene crystallographically aligned with a hexagonal boron nitride, we report various kinds of symmetry-breaking transition tuned by displacement fields (D) and magnetic fields: (i) While it is well known that a finite D can enhance correlation to result in correlated insulators at fractional fillings of a flat band, we find the correlation gap emerges before the flavor is fully filled at a positive D, but the sequence is reversed at a negative D. (ii) Around zero D, electronic correlation can be invoked by narrow Landau levels, leading to quantum Hall ferromagnetism that lifts all the degeneracies including not only spin and valley but also orbital degrees of freedom. Our result unveils the complication of transitions between symmetry-breaking phases, shedding light on the mechanisms of various exotic phenomena in strongly correlated systems.

Keywords: rhombohedral trilayer graphene, moiré superlattice, symmetry breaking, flavor polarization, van Hove singularity, quantum Hall ferromagnetism

PACS: 72.80.Vp, 73.40.–c, 73.21.Cd **DOI:** 10.1088/1674-1056/acddcf

1. Introduction

Exotic quantum phases including superconductivity, ferromagnetism, and Chern insulators emerge at the moiré interface that hosts strongly correlated electrons.[1–13] The key may lie in the fact that electronic correlation results in flavor symmetry breaking between spin and valley degrees of freedom,[14–20] owing to fulfillment of the Stoner criteria $\rho U > 1$, where ρ is density of states (DOS) on the Fermi surface and U is the on-site energy. With the lifted degeneracy, for example, electrons residing at only one of K and $-K$ valleys, orbital magnetic moment with broken time reversal symmetry would arise, leading to ferromagnetism and a nonzero Chern number.[21] While the origin of superconductivity so far has been highly debated,[1,2,22–25] the universal observation of superconductivity close to transition boundaries of non-degenerate phases implies its inherent connection to isospin fluctuation,[26] mimicking the antiferromagnetic spin fluctuation in cuprate. As a result, it is of high interest to investigate how the symmetry is broken at fractional commensurate fillings of the flat moiré band. In twisted bilayer graphene, both transport and thermodynamic measurement[14,17,19,20,27] reveal that carriers tend to reset at integer multiple of full filling of one flavor, i.e., carriers of all partially filled flavors turn into a specific flavor to make the latter fully filled; Since the full flavor cannot contribute to electric conduction, the mobile carrier density is reset to zero. During the whole process, the carrier type, nevertheless, is unchanged. By contrast, in twisted mono-bilayer graphene,[28–31] there are different types of carriers (electrons and holes) on the two sides of the phase boundary, which infers that a new band edge (stemming from the phase transition and the associated energy gap) emerge before the commensurate filling. Such detailed difference may reflect the delicate energy competition between various ground states in different moiré systems, which in turn controls the aforementioned exotic phenomena.

In this work, by studying zero-degree twisted rhombohedral trilayer graphene (ABC-TLG) and hexagonal boron nitride, we find distinct symmetry-breaking transitions coexisting in the same sample but depending on the direction of displacement fields. At fractional fillings of the moiré band, a correlation gap can be observed before the flavors are fully filled at a positive D, but at a negative D it does not emerge until the commensurate filling is achieved. In addition, in the

[†]Corresponding author. E-mail: hanchunrui@ime.ac.cn
[‡]Corresponding author. E-mail: jmlu@pku.edu.cn

© 2023 Chinese Physical Society and IOP Publishing Ltd

proximity of zero D flavor symmetry breaking is found to be invoked by a strong magnetic field, owing to the narrow bandwidth of Landau levels. The quantum Hall ferromagnetism, as expected, lifts spin, valley, and even orbital degeneracies. Our work demonstrates a rhombohedral trilayer graphene superlattice as a good platform to investigate correlation-induced symmetry breaking at phase boundaries, paving the way to tune quantum phases in strongly correlated systems.

2. Results

Pristine trilayer graphene flakes are micromechanically exfoliated onto silicon wafers from natural graphite. The rare rhombohedral part is distinguished from Bernal trilayer graphene by Raman spectrum of two-dimensional (2D) peaks at 2700 cm^{-1}.[32,33] Then it is encapsulated by hexagonal boron nitride (hBN) flakes with the top hBN crystallographically aligned, and a moiré superlattice is formed as a result of the small lattice mismatch between graphene and hBN crystals (see schematics in the inset of Fig. 1(a), where the superlattice unit cell and lattice constant λ are depicted). The measurement scheme is illustrated in Fig. 1(a), where the top gate V_t and the bottom gate V_b are used to tune the carrier density n and displacement field D independently. The definition is as follows: $n = D_b + D_t$, $D = (D_b - D_t)/2$, with $D_{b(t)} = \varepsilon_0\varepsilon_r V_{b(t)}/d_{b(t)}$, ε_r is the relative dielectric constant of hBN, $d_{b(t)}$ is the thickness of the bottom (top) hBN flake. For convenience, we further define $\nu_s = 4n/n_s$, where n_s is the carrier density accommodated by the moiré band.

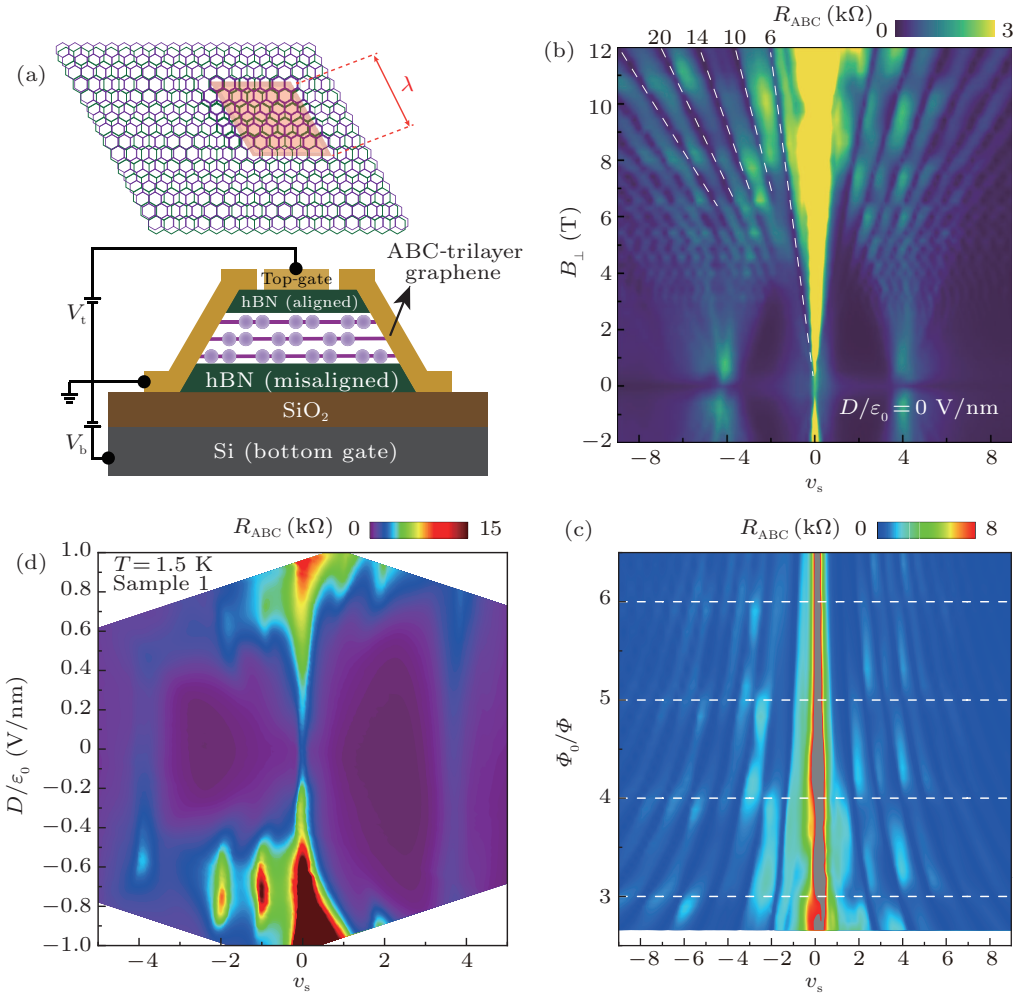


Fig. 1. The electronic phase diagram. (a) schematic diagram of the device measurement. Left inset: Atomic model of a rhombohedral trilayer graphene and a sketch of moiré superlattices, in which a superlattice unit cell with lattice constant λ is highlighted. (b) At $D = 0$ V/nm, Landau level fans stem from both CNP and two FFP, showing clear Brown–Zak oscillation. (c) Derivation of twist angle as 0.2°. (d) The D–ν_s phase diagram, where correlated insulators at $\nu_s = \pm 1$ and ± 3 are observed in both conduction and valence moiré bands. However, the range of displacement fields for each correlated insulator is distinct.

To determine the twist angle between graphene and the top hBN flake, Hall carrier density is measured to obtain the gate capacitance and thus electron concentration of full filling of moiré bands n_s can be obtained. As n_s is directly related with λ (the inset of Fig. 1(a)), we finally obtain the superlattice constant and twisted angle. A more precise method is shown in Figs. 1(b) and 1(c), in which Landau fan at $D = 0$ V/nm shows significant Brown–Zak oscillation[34–36] and we can fit

the superlattice constant as 12.4 nm. Using formula[37]

$$\lambda = \frac{(1+\delta)\,a}{\sqrt{2\,(1+\delta)\,(1-\cos\theta)+\delta^2}},$$

where $a = 2.464$ Å is the graphene lattice constant, $\delta = 0.018$ is the lattice difference between hBN and graphene, we get the twist angle θ as 0.2°. The result agrees with the Hall effect shown in Fig. 2, where at full filling of the moiré band $n_{\rm H} = 3\times10^{12}$ cm^{-2} is obtained and the derived λ from the formula $1/n = \sqrt{3}\lambda^2/8$ is 12.41 nm. With these parameters, one can plot the phase diagram as a function of D and $\nu_{\rm s}$ in Fig. 1(d). At $\nu_{\rm s} = 0$ (charge neutral point, CNP), resistance increase fast with increasing $|D|$. The D-sensitive bandgap opening is consistent with the rhombohedral stacking order of a trilayer graphene.[38,39] At $\nu_{\rm s} = \pm4$, resistance peaks indicate the superlattice gap is generated, but is smaller than that of CNP in magnitude. In between, correlated insulators at $\nu_{\rm s} = -1$, -2 can be observed at both positive and negative displacement fields,[10–13] but their specific ranges of D are different. The strong D dependence suggests that intrinsic properties are also effectively tuned by D fields, such as van Hove singularity (the origin of electronic correlation) and flavor polarization.

3. Distinct flavor polarization at positive and negative D

In Fig. 2(a), we map the filling factor derived from antisymmetrized Hall signal $\nu_{\rm H} = 4n_{\rm H}/n_{\rm s}$, where $n_{\rm H} = -1/(eR_{\rm H})$. The definition of VHS is $R_{\rm H} = 0$, which means the nominal density $\nu_{\rm H}$ at VHS is divergent.[31] In other words, $\nu_{\rm H}$ in adjacent to VHS is either positive or negative infinity, which can be identified by transition from deep blue to deep red as shown in the inset of Fig. 2(b). In addition, there are two other types: one is bandgap, the other is carrier reset. The former stands for carriers evolving gradually from electron to hole with zero net carriers in the middle, so that the color changes from light blue to light red. The latter is similar, but without changing carrier type: $\nu_{\rm H}$ firstly decreases to zero (or a finite value in practical experiment) then rises again. Consequently, during the transition the color changes into white then blue/red again. Based on these categorizations,[2] we get a schematic diagram in Fig. 2(b).

Similar to many multilayer graphene like twisted mono-bilayer graphene[28–31] and twisted double bilayer graphene,[40–42] the VHS has a close relationship with D. An interesting feature of VHS is the significant jump: in the low-D regime VHS is located very close to the full filling point of the moiré band (FFP), however, it jumps to the vicinity of CNP at relatively large D where correlated insulators emerge. As a result, in the broad regime with strong correlation, the carrier type in the valence moiré band is electron-like rather than hole-like.

A more interesting feature in Fig. 2(b) is the contrasting behavior between positive and negative displacement fields. For correlated insulators at commensurate fillings ($\nu_{\rm s} = -1$, -2), at positive D there are correlated gaps (blue), but at negative D they are reset (magenta). To check the details, we select $D = \pm0.6$ V/nm and plot filling factor $\nu_{\rm H}$ (right axis) and Hall resistance $R_{\rm H}$ (left axis) in Figs. 2(c)–2(d), respectively. Corresponding to the colored lines in Fig. 2(b), shaded regions are highlighted. Obviously, in Fig. 2(c) the correlated gap of $\nu_{\rm s} = -2$ must emerge before $\nu_{\rm s}$ reaches -2, because at $\nu_{\rm s} = -1.5$ a new band edge already appears and the sign of the band curvature (hence carrier type) is changed to be opposite owing to the correlated gap. In contrast, in Fig. 2(d) the carrier type is always electron when $\nu_{\rm s}$ passes VHS at -0.5 V/nm, indicating that the flavor polarization and correlated gap at $\nu_{\rm s} = -1$, -2 only appear when $\nu_{\rm s}$ reaches -1 and -2. Following the Stoner criteria, DOS (ρ) and/or U seems to be greater at a positive D than a negative D, so that the flavor polarization can occur earlier in the former. However, in Fig. 1(d) stronger correlated insulator at a negative D suggests a larger U. In general, a positive D would push electrons to the bottom layer of ABC-TLG. The holes reside further away from the moiré interface for a positive D than a negative D, thus the latter is experiencing stronger potential modulation from the top hBN. As a result, the negative D has a larger superlattice bandgaps at $\nu_{\rm s}$, i.e., the band is better isolated. Without band isolation, the thermally excited or disorder-scattered carriers from the lower bands would suppress the ordering of the electrons and hence the correlated states,[43] which may explain the more resistive correlated peak at a negative D. Whether the stronger modulation further flattens the moiré band at the negative D remains in debate.[15,44] We leave the question about which D has a larger U to the future.

At last, we would like to propose a filling sequence for each case. In general, there are two kinds of moiré superlattice, one is thought to be strong modulation in homo-bilayer such as twisted bilayer graphene, the other is weak modulation from distinct constituent layers such as graphene and hBN heterostructures. In the latter systems, e.g., a rhombohedral trilayer graphene superlattice studied in this work, moiré potential is suggested to play a minor role in determining electronic ground states.[15] It was shown that in pristine trilayer graphene, due to the strong electron-correlation induced flavor polarization, the filling sequence is a single spin–valley polarized flavor at the beginning, then two valleys of the same spin and finally four degenerate flavors.[15] So in the cartoon on top of both Figs. 2(c) and 2(d), we follow such a filling sequence, but with a difference of when the correlated gap emerges. Note that here electron and holes are denoted by red and blue colors, respectively. To represent the carrier type on the Fermi surface, deep red/blue are used; In other scenarios, e.g., a fla-

vor is fully filled by electron/hole, light red/blue are plotted.

The above picture is based on the capacitance measurement results[15] of both moiré superlattice and moiréless ABC-TLG, where one can assume that the moiré potential modulation does not change flavor symmetry-breaking phases in its moiréless counterpart. The assumption is also supported by the observation of Chern number $C = -2$, 0 at $\nu = -1$, -2, respectively.[11] The former indicates the population of a single spin–valley flavor, coinciding with the quarter metal; the latter means the occupation of valley-unpolarized flavors, consistent with the spin-polarized half metal. However, direct verification of the nature of flavor polarization, which needs a high-quality sample to observe quantum oscillation, is yet to be realized.[15] Such an effort deserves more investigation, because recent theories raised a distinct point of view:[44] The graphene/hBN superlattice should not be described by weakly coupled itinerant electrons that exhibit flavor polarization and band reconstruction by the moiré potential; in contrary, a strong-coupling renormalization of electronic band is required.

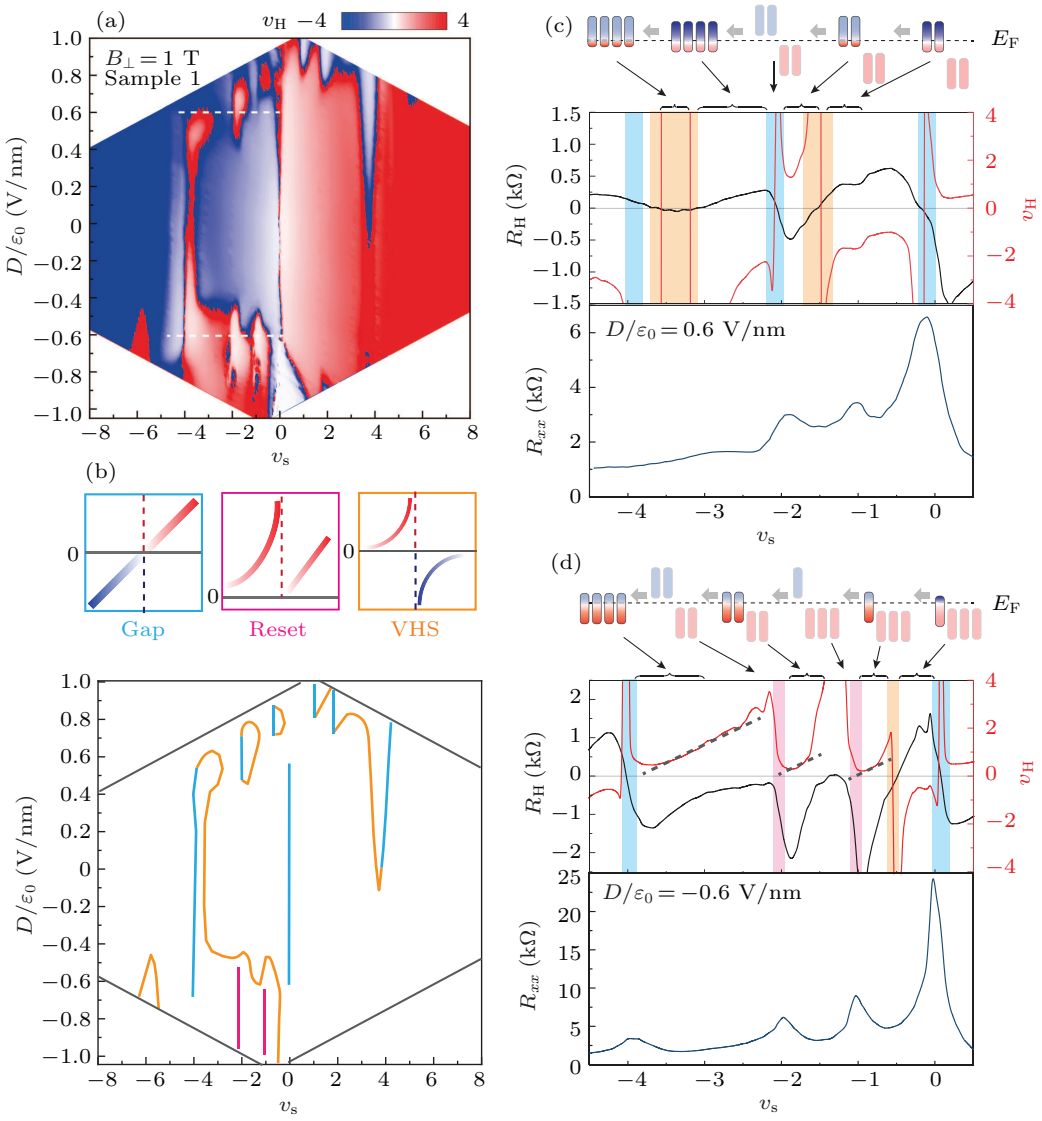


Fig. 2. Two types of flavor polarization and distorted van Hove singularity: (a) filling factors ν_H derived from Hall effects over the whole phase diagram. Within moiré bands ($-4 < \nu_s < 4$), van Hove singularity (denoted by the boundary between deep blue and deep red) is close to FFP at a low displacement field, but jumps abruptly to the vicinity of CNP at a high displacement field where correlated insulators take place. (b) Schematic plot of van Hove singularity (yellow), carrier reset (magenta), and band-/correlated gaps (blue) in the phase diagram, whose definitions are depicted in the insets. (c)–(d) Corresponding to the two white-dashed lines in panel (a), filling factor (ν_H on the right axis) and Hall resistance (R_H on the left axis) at $D = 0.6$ V/nm (c) and -0.6 V/nm (d) are plotted, where the three types of features defined in panel (b) are highlighted. Evolution of flavor population is schematically shown on the top, where blue and red colors represent holes and electrons, respectively. Longitudinal resistance is also attached at the bottom panel.

4. Quantum Hall ferromagnetism driven by electric fields

Similar to van Hove singularity, Landau levels may also lead to a substantial density of states. Following the Stoner criteria $\rho U > 1$, both can invoke flavor polarization because of the gain in exchange exceeding the cost in kinetic energy. Mimicking the spin polarization induced ferromagnetism, flavor polarization within LLs is termed as quantum Hall ferromagnetism.[45,46]

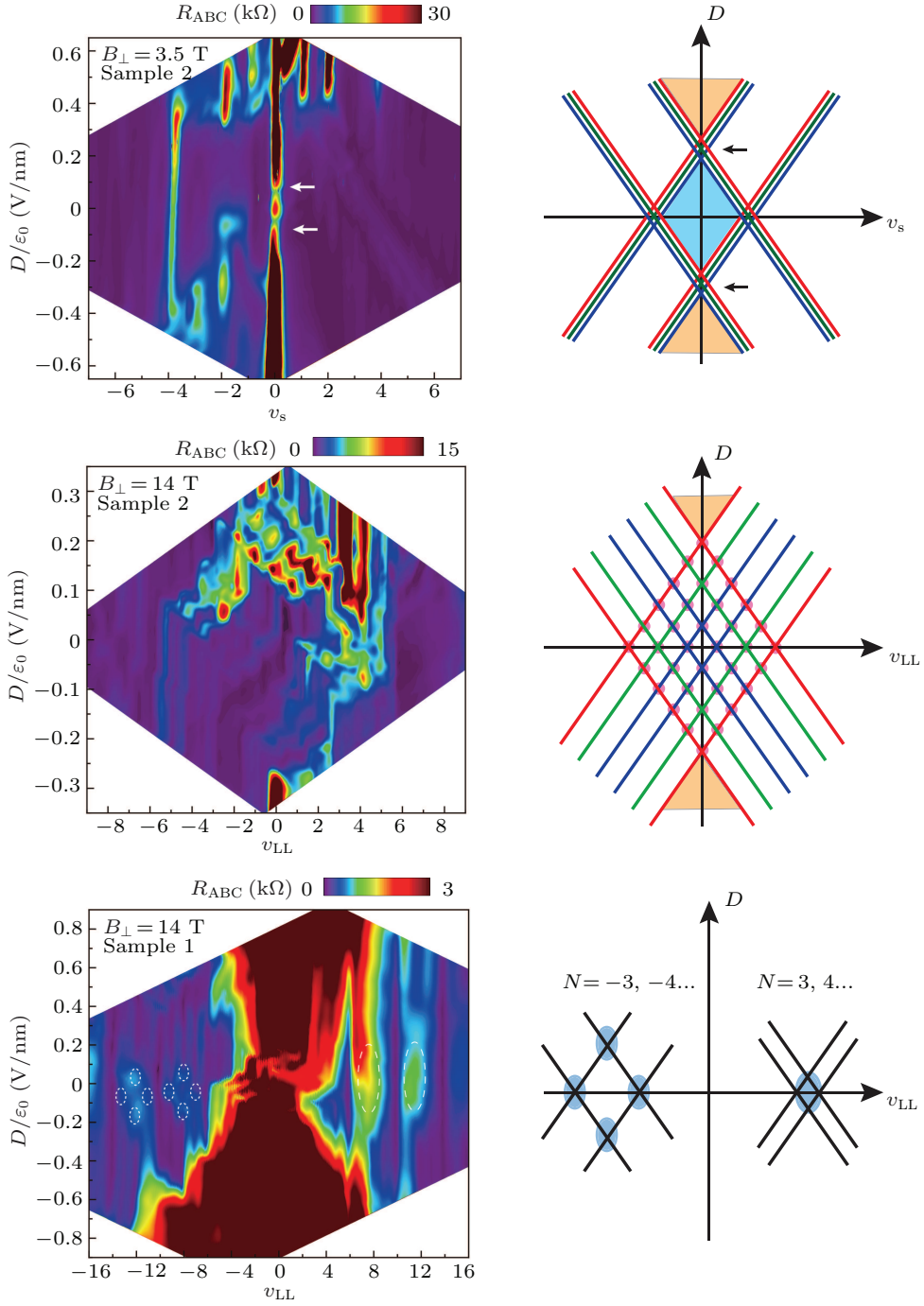


Fig. 3. Quantum Hall ferromagnetism: (a) At a small magnetic field, an increasing displacement field drives the spin-to-valley polarization for the first three LLs. The transition points are denoted by white arrows in the left phase diagram and black arrows in the right schematics. Note that the degenerate orbitals $N = 0$, 1, 2 LLs are represented by different colors. (b) A strong magnetic field further break the orbital degeneracy between $N = 0$, 1, 2 LLs, resulting in a matrix-like pattern. (c) For $|N| > 2$, a typical spin-to-valley polarization is usually observed, except when the spin gap on the electron side is blurred by thermal fluctuation. Cross points are denoted by white dashed ellipses on the left and by shaded ellipses on the right.

Here in a rhombohedral trilayer graphene, LLs' energies follow:[46–49] $E_N = \pm[(2\hbar v_F eB)^{3/2})/(\gamma_1^2)][N(N-1)(N-2)]^{1/2}$, where N is an integer denoting the LL index, e is the electron charge, $v_F \sim 10^6$ m/s is the Fermi velocity of single layer graphene, γ_1 is the interlayer hopping energy, and h is Planck's constant. Without correlation induced symmetry breaking, LLs of $N = 0$, 1, and 2 are degenerate. Including the spin and valley degrees of freedom, it yields a 12-fold degeneracy for the lowest LL. This is exactly what we observe in Fig. 3(a). At $B = 3.5$ T, the energy interval between LLs is, to some extent, smeared by disorder and thermal fluctuation, thus the overlap of broadened LLs reduces the electronic correlation. As a result, the orbital degeneracy for $N = 0$, 1, 2 is preserved. In contrast, the spin degeneracy is lifted by the B field and the valley degeneracy is broken by the D field. The latter is due to that valley degree of freedom is locked to layers in real space for zeroth Landau levels in graphene. Obviously, at $D = 0$ V/nm the gapped ground state at CNP is spin-

polarization (blue shaded region in the right panel of Fig. 3(a)); with increasing D the LLs cross each other and enters into another gapped state that is of valley polarization (shaded in yellow). Such a spin-to-valley polarization transition is also observed for a larger orbital number $N > 2$, in which the total degeneracy is four hence the mechanism is straightforward (Fig. 3(c)). Note that in Figs. 3(c) and 3(d), instead of ν_s we use the Landau level filling index $\nu_{LL} = n/(B/\Phi_0)$, where Φ_0 is flux quanta.

The D-driven spin-to-valley polarization becomes more complicated when more symmetry breaking is involved. As shown in Fig. 3(b), the increasing B field renders an LL further apart in energy from adjacent LLs, hence electronic correlation is enhanced. A direct result is the lifting of orbital degeneracy. The simple line crossing (Fig. 3(a)) now becomes a matrix (Fig. 3(b)).

5. Discussion

In this work, various symmetry-breaking processes between spin and valley flavors are unveiled in a rhombohedral trilayer graphene superlattice. When the displacement field is sufficiently large, the flattened band dispersion is enough to give rise to an ultrahigh density of states to fulfill the requirement of Stoner criteria. Consequently, we can observe spontaneous symmetry breaking and flavor polarization. Around zero D, however, one needs to introduce Landau levels of narrow bandwidth to break spin, valley, and orbital degeneracies. Despite the common points for all the transitions, we note that the different details provide valuable insight to the process of when and how the flavor symmetry is broken. Such information is expected to help understand the ground states of exotic quantum phases in fast growing Moiré superlattice systems.

Acknowledgements

Project supported by the National Natural Science Foundation of China (Grant Nos. 11974027 and 62275265), the National Key Research and Development Program of China (Grant Nos. 2019YFA0307800 and 2021YFA1400100), and Beijing Natural Science Foundation (Grant Nos. Z190011 and 4222084).

References

[1] Cao Y, Fatemi V, Fang S, Watanabe K, Taniguchi T, Kaxiras E and Jarillo-Herrero P 2018 *Nature* **556** 43
[2] Park J M, Cao Y, Watanabe K, Taniguchi T and Jarillo-Herrero P 2021 *Nature* **590** 249
[3] Hao Z, Zimmerman A M, Ledwith P, Khalaf E, Najafabadi D H, Watanabe K, Taniguchi T, Vishwanath A and Kim P 2021 *Science* **371** 1133
[4] Park J M, Cao Y, Xia L Q, Sun S, Watanabe K, Taniguchi T and Jarillo-Herrero P 2022 *Nat. Mater.* **21** 877
[5] Cao Y, Fatemi V, Demir A, Fang S, Tomarken S L, Luo J Y, Sanchez-Yamagishi J D, Watanabe K, Taniguchi T, Kaxiras E, Ashoori R C and Jarillo-Herrero P 2018 *Nature* **556** 80
[6] Sharpe A L, Fox E J, Barnard A W, Finney J, Watanabe K, Taniguchi T, Kastner M A and Goldhaber-Gordon D 2019 *Science* **365** 605
[7] Serlin M, Tschirhart C L, Polshyn H, Zhang Y, Zhu J, Watanabe K, Taniguchi T, Balents L and Young A F 2020 *Science* **367** 900
[8] Wu S, Zhang Z, Watanabe K, Taniguchi T and Andrei E Y 2021 *Nat. Mater.* **20** 488
[9] Das I, Lu X, Herzog-Arbeitman J, Song Z D, Watanabe K, Taniguchi T, Bernevig B A and Efetov D K 2021 *Nat. Phys.* **17** 710
[10] Chen G, Jiang L, Wu S, Lyu B, Li H, Chittari B L, Watanabe K, Taniguchi T, Shi Z, Jung J, Zhang Y and Wang F 2019 *Nat. Phys.* **15** 237
[11] Chen G, Sharpe A L, Fox E J, Zhang Y H, Wang S, Jiang L, Lyu B, Li H, Watanabe K, Taniguchi T, Shi Z, Senthil T, Goldhaber-Gordon D, Zhang Y and Wang F 2020 *Nature* **579** 56
[12] Chen G, Sharpe A L, Gallagher P, Rosen I T, Fox E J, Jiang L, Lyu B, Li H, Watanabe K, Taniguchi T, Jung J, Shi Z, Goldhaber-Gordon D, Zhang Y and Wang F 2019 *Nature* **572** 215
[13] Yang J, Chen G, Han T, Zhang Q, Zhang Y-H, Jiang L, Lyu B, Li H, Watanabe K, Taniguchi T, Shi Z, Senthil T, Zhang Y, Wang F and Ju L 2022 *Science* **375** 1295
[14] Park J M, Cao Y, Watanabe K, Taniguchi T and Jarillo-Herrero P 2021 *Nature* **592** 43
[15] Zhou H, Xie T, Ghazaryan A, Holder T, Ehrets J R, Spanton E M, Taniguchi T, Watanabe K, Berg E, Serbyn M and Young A F 2021 *Nature* **598** 429
[16] de la Barrera S C, Aronson S, Zheng Z, Watanabe K, Taniguchi T, Ma Q, Jarillo-Herrero P and Ashoori R 2022 *Nat. Phys.* **18** 771
[17] Zondiner U, Rozen A, Rodan-Legrain D, Cao Y, Queiroz R, Taniguchi T, Watanabe K, Oreg Y, von Oppen F, Stern A, Berg E, Jarillo-Herrero P and Ilani S 2020 *Nature* **582** 203
[18] Seiler A M, Geisenhof F R, Winterer F, Watanabe K, Taniguchi T, Xu T, Zhang F and Weitz R T 2022 *Nature* **608** 298
[19] Saito Y, Yang F, Ge J, Liu X, Taniguchi T, Watanabe K, Li J I A, Berg E and Young A F 2021 *Nature* **592** 220
[20] Rozen A, Park J M, Zondiner U, Cao Y, Rodan-Legrain D, Taniguchi T, Watanabe K, Oreg Y, Stern A, Berg E, Jarillo-Herrero P and Ilani S 2021 *Nature* **592** 214
[21] Liu J and Dai X 2021 *Nat. Rev. Phys.* **3** 367
[22] Cao Y, Park J M, Watanabe K, Taniguchi T and Jarillo-Herrero P 2021 *Nature* **595** 526
[23] Stepanov P, Das I, Lu X, Fahimniya A, Watanabe K, Taniguchi T, Koppens F H L, Lischner J, Levitov L and Efetov D K 2020 *Nature* **583** 375
[24] Saito Y, Ge J, Watanabe K, Taniguchi T and Young A F 2020 *Nat. Phys.* **16** 926
[25] Liu X, Wang Z, Watanabe K, Taniguchi T, Vafek O and Li J I A 2021 *Science* **371** 1261
[26] Zhou H, Xie T, Taniguchi T, Watanabe K and Young A F 2021 *Nature* **598** 434
[27] Wong D, Nuckolls K P, Oh M, Lian B, Xie Y, Jeon S, Watanabe K, Taniguchi T, Bernevig B A and Yazdani A 2020 *Nature* **582** 198
[28] Polshyn H, Zhu J, Kumar M A, Zhang Y, Yang F, Tschirhart C L, Serlin M, Watanabe K, Taniguchi T, MacDonald A H and Young A F 2020 *Nature* **588** 66
[29] Chen S, He M, Zhang Y H, Hsieh V, Fei Z, Watanabe K, Taniguchi T, Cobden D H, Xu X, Dean C R and Yankowitz M 2021 *Nat. Phys.* **17** 374
[30] He M, Zhang Y H, Li Y, Fei Z, Watanabe K, Taniguchi T, Xu X and Yankowitz M 2021 *Nat. Commun.* **12** 4727
[31] Xu S, Al Ezzi M M, Balakrishnan N, Garcia-Ruiz A, Tsim B, Mullan C, Barrier J, Xin N, Piot B A, Taniguchi T, Watanabe K, Carvalho A, Mishchenko A, Geim A K, Fal'ko V I, Adam S, Neto A H C, Novoselov K S and Shi Y 2021 *Nat. Phys.* **17** 619
[32] Lui C H, Li Z, Chen Z, Klimov P V, Brus L E and Heinz T F 2011 *Nano Lett.* **11** 164
[33] Ding D, Niu R, Han X, Qu Z, Wang Z, Li Z, Liu Q, Han C and Lu J 2023 *Chin. Phys. B* **32** 067204
[34] Krishna Kumar R, Chen X, Auton G H, Mishchenko A, Bandurin D A, Morozov S V, Cao Y, Khestanova E, Ben Shalom M, Kretinin A V, Novoselov K S, Eaves L, Grigorieva I V, Ponomarenko L A, Fal'ko V I and Geim A K 2017 *Science* **357** 181
[35] Krishna Kumar R, Mishchenko A, Chen X, Pezzini S, Auton G H, Ponomarenko L A, Zeitler U, Eaves L, Fal'ko V I and Geim A K 2018 *Proc. Natl. Acad. Sci. USA* **115** 5135

[36] Barrier J, Kumaravadivel P, Krishna Kumar R, Ponomarenko L A, Xin N, Holwill M, Mullan C, Kim M, Gorbachev R V, Thompson M D, Prance J R, Taniguchi T, Watanabe K, Grigorieva I V, Novoselov K S, Mishchenko A, Fal'ko V I, Geim A K and Berdyugin A I 2020 *Nat. Commun.* **11** 5756

[37] Yankowitz M, Xue J, Cormode D, Sanchez-Yamagishi J D, Watanabe K, Taniguchi T, Jarillo-Herrero P, Jacquod P and LeRoy B J 2012 *Nat. Phys.* **8** 382

[38] Lui C H, Li Z, Mak K F, Cappelluti E and Heinz T F 2011 *Nat. Phys.* **7** 944

[39] Zou K, Zhang F, Clapp C, MacDonald A H and Zhu J 2013 *Nano Lett.* **13** 369

[40] Liu X, Hao Z, Khalaf E, Lee J Y, Ronen Y, Yoo H, Haei Najafabadi D, Watanabe K, Taniguchi T, Vishwanath A and Kim P 2020 *Nature* **583** 221

[41] He M, Li Y, Cai J, Liu Y, Watanabe K, Taniguchi T, Xu X and Yankowitz M 2021 *Nat. Phys.* **17** 26

[42] Shen C, Chu Y, Wu Q, Li N, Wang S, Zhao Y, Tang J, Liu J, Tian J, Watanabe K, Taniguchi T, Yang R, Meng Z Y, Shi D, Yazyev O V and Zhang G 2020 *Nat. Phys.* **16** 520

[43] Cao Y, Rodan-Legrain D, Rubies-Bigorda O, Park J M, Watanabe K, Taniguchi T and Jarillo-Herrero P 2020 *Nature* **583** 215

[44] Patri A S and Senthil T 2023 *Phys. Rev. B* **107** 165122

[45] Lee K, Fallahazad B, Xue J, Dillen D C, Kim K, Taniguchi T, Watanabe K and Tutuc E 2014 *Science* **345** 58

[46] Lee Y, Tran D, Myhro K, Velasco J Jr, Gillgren N, Poumirol J M, Smirnov D, Barlas Y and Lau C N 2016 *Nano Lett.* **16** 227

[47] Yin L J, Shi L J, Li S Y, Zhang Y, Guo Z H and He L 2019 *Phys. Rev. Lett.* **122** 146802

[48] Zhang L, Zhang Y, Camacho J, Khodas M and Zaliznyak I 2011 *Nat. Phys.* **7** 953

[49] Bao W, Jing L, Velasco J, Lee Y, Liu G, Tran D, Standley B, Aykol M, Cronin S B, Smirnov D, Koshino M, McCann E, Bockrath M and Lau C N 2011 *Nat. Phys.* **7** 948